Application of computer image processing technology in old artistic design restoration

Guo Chen [a],[*], Zhiyong Wen [b], Fazhong Hou [b],[**]

[a] *James Cook University Singapore Campus, 387380, Singapore*
[b] *Hubei University of Arts and Science, Xiangyang, 441053, China*

ARTICLE INFO

ABSTRACT

Art designs exhibit different principles, textures, color combinations, and creative skills for vivid thinking visualizations. Art exhibits are far from ages, periods, and creators finding their digital patterns in recent years for resurrection. Degraded periodic artworks are digitally handled for reviving their legacy using digital image processing. This article introduces Textural Restoration Technique (TRT) using Deep Feature Processing (DFP) to augment such innovations. The proposed technique analyses the tampered image for its textures, and available features are extracted. The textures are expected to be sequential based on gradient distribution; the missing gradients are identified from the available features near the region of interest (ROI). The ROI is marked by combining missing and available features from which textural edges are sketched. In this process, recurrent learning is employed for verifying the gradient substitutions for even textures. The texture patterns are classified using high and low accuracy features exhibited between two successive ROIs. First, the learning model is trained using gradient distribution accuracy pursued by the texture completion edge. The second training is pursued by the first distribution, achieving the maximum restoration. The filled features and their gradient positions are marked by moving the ROIs for distinguishing textures. The restoration ratio is computed with high accuracy based on the filled edges.

1. Introduction

Computer image processing is done in digital computers to process images using algorithms. The actual goal of image processing is to identify the patterns and characteristics of an image [1–3]. Computer image processing technique is used for art design, improving design capabilities. Image processing reduces the complexity ratio in the art designing process. Art designing requires proper data and features gathered from various databases and networks [4]. In art design, digital image processing (DIP) technology identifies an image's important patterns and scene values. DIP technique detects the exact content required for the art designing process [5]. DIP uses machine learning algorithms that improve the efficiency of image processing systems. Visual communication is a part of arts that first analyses the features and factors for design [6]. Computer image processing is used in visual communication, which uses an analysis technique that identifies the key elements and types of patterns. Computer image processing also detects the color, feature, space, words, and factors for art design [7–10].

Art design pattern analysis is a process that analyzes the patterns for art design. Design pattern analysis is a complicated task in every art designing system. Heterogeneous features are widely used for pattern recognition and analysis [11,12]. Heterogeneous features are commonly used for multimedia analysis and designing systems. Pattern analysis identifies key values, dimensions, high-quality features, and details [13,14]. Heterogenous features use transfer learning algorithms that characterize the sources and domains based on features and functions. Heterogenous features are calculated using the feature selection method [15–17]. The selection method assimilates the necessary features that provide accurate data for the art design pattern detection process. The feature selection method increases the accuracy of pattern analysis, enhancing the efficiency and performance ratio in art designing processes [18,19]. An automatic pattern detection method is also used for the art design pattern analysis process. Heterogenous features reduce the latency and energy consumption range in pattern analysis and detection processes. The heterogeneous features-based detection method predicts the actual and accurate features for design patterns [20,21].

Machine learning (ML) algorithms and techniques are widely used for detection and prediction processes. ML algorithms maximize the overall accuracy of the detection process. ML algorithm is used for the art image pattern detection process [22]. Convolution neural network is common in identifying patterns from heterogeneous images. CNN algorithm uses a feature selection method that extracts the important features from the image [23]. The CNN algorithm detects the patterns and features presented in images and pictures. CNN algorithms collect the relevant data from the database, reducing the latency in classification and identification processes [24]. A deep reinforcement learning algorithm (DRL) based method is also used for image pattern detection. The DRL algorithm uses the detection method to evaluate the sophisticated features presented in an image [25]. The DRL-based detection method achieves high accuracy in image pattern detection. The DRL algorithm recognizes the factors and patterns from the images that produce relevant data for further analysis [26]. The prime highlights of the article are listed below:

❖ Introducing a texture-based old artistic image restoration technique by identifying the region of interest and gradient distribution process.
❖ Including a deep learning-based classification process for identifying different textural patterns and feature analysis for mitigating false positives.
❖ Performing a comparative analysis using specific metrics and methods for validating the proposed techniques' performance.

The rest of the article has been prepared: section 2 discusses the related works, section 3 proposes the TRT-DFP model, section 4 deliberates the results and discussion, and section 5 concludes the research article.

2. Related works

Hatir and Ince [27] proposed a stone heritage mapping model using a region-based convolutional neural network (R–CNN). The main aim of the proposed model is to prevent human errors in cultural heritage properties. The exact stone types and classes are detected from the historic building, reducing the error ratio in the analysis processes. The r-CNN technique reduces the energy consumption range in the computation process. The proposed mapping model maximizes the lithology determination of prevention processes.

Jin et al. [28] introduced a deep convolutional neural network (CNN) framework for image restoration. CNN framework identifies the important values and characteristics of artifacts from the given images. Residual learning is implemented here to train the datasets for further processes. Training parameters and variables are also detected from the database, reducing the restoration process's latency. The introduced CNN framework improves flexibility and maximizes the performance range of image restoration systems.

Yuan and He [29] designed a randomized image transformation method using an adversarial deep neural network (DNN) for attacked image restoration. The actual goal is to recover the original image from the attacked images. A target classifier is used here to classify images' important patterns and pixels. The DNN detects the noises presented in the image and eliminates the unwanted data

Table 1
Summary of references [32–36].

Author	Title	Process	Results
Farajzadeh and Hashemzadeh [32]	A deep artificial neural network (ANN) based image inpainting approach for image restoration.	Irregular structures and unwanted noises which are presented in the images are removed by ANN.	ANN predicts the exact colors and restores the damaged images.
Li et al. [33]	A non-convex hybrid regularization model for blurred image restoration.	Both multiplicative and addictive noises are removed from the images.	Maximizes accuracy and reduces the error in the blurred image restoration process.
Chen et al. [34]	An L0 regularized cartoon-texture model for blurred and corrupted image restoration.	Image deblurring technique is used here to deblur the corrupted image, reducing the latency in the restoration process.	Impulsive noises are also removed from the image, enhancing the image restoration efficiency ratio.
Wang et al. [35]	An optimization method for motion blur image restoration	Texture mapping is used here to deblur the image, providing relevant data for further processes.	Reduces the latency ratio in ringing artifacts, which maximizes the robustness of the systems.
Wu et al. [36]	A systematic approach to the image restoration process.	Iterative regularization is used here as a strategy to restore the damaged and attacked images.	The proposed approach achieves high accuracy in the image restoration process.

from the attacked image. Experimental results show that the introduced method achieves high accuracy in the image recovery process.

Xue et al. [30] developed a local transformer with a spatial partition restore network (SPRLT-Net) for hyperspectral image classification (HIC). The main aim of the proposed method is to obtain the spatial partition presented in the images. The transformers detect the original patches and pixels of the images, reducing the energy consumption ratio in the computation process. Compared with other methods, the developed SPRLT-Net maximizes the accuracy in image classification, enhancing the generalization performance efficiency.

Wan et al. [31] proposed a novel triplet-domain translation network for image restoration. Variational autoencoders (VAEs) are used here to transform the old photos and to clean the damaged parts of the photos. A deep latent space translation is used here to identify old photos' patterns and pixel rates. VAE compares the old photo with the new one, which produces the necessary information for the image restoration process. The proposed network increases the old image restoration process's overall quality and effectiveness range. references [32–36] are shortly summarized in Table 1 for ease of similar method understanding.

Lee and Kang [37] proposed a sparse representation-based variational model for blurred image restoration. The actual goal of the model is to recover the blurred images with Cauchy noises. Cauchy noises and blurriness presented in the images are eliminated from the given images. An optimization scheme is used to identify the exact features and key values from the images. Experimental results show that the proposed model outperforms the image restoration process.

Kang and Jung [38] introduced a non-convex total variation for image restoration. The introduced method is a proximal alternating minimization approach that solves optimization problems. An alternating minimization algorithm is used here to detect the illumination content from the images. The noises and blurriness of the images are identified and removed during the image restoration process. The introduced method increases the overall accuracy of image restoration systems.

Zamir et al. [39] developed an efficient transformer model for high-resolution image restoration. A convolutional neural network (CNN) algorithm is used in the model to detect the prior features from the image patterns. The CNN algorithm analyzes the information from large-image pixels, enhancing restoration tasks' effectiveness. The developed model improves the performance range of the image restoration process.

Wang et al. [40] proposed a U-shaped transformer (uformer) for image restoration systems. The main aim of the model is to restore the core details from low-resolution images. The images' spatial and temporal features are selected for the restoration process. It also evaluates the gap between the features and provides accurate information for further processes. The proposed former model increases the accuracy level of image restoration.

Kumar and Gupta [41] introduced a generative adversarial network-based image restoration method for damaged artworks. A unique image restoration method restores the images using complex features. The adversarial network generates physical changes to damaged artworks. The introduced method reduces both time and energy consumption levels in the computation process. The introduced method improves the performance ratio of the image restoration process.

The proposed technique differs from the texture-based approaches in Refs. [34,35] by preventing unnecessary mapping for the extracted features. Region-dependent methods, as in Ref. [27], and irregularity-suppressing methods, as in Refs. [28,32], cause more complexity due to uneven distributions. Considering the variations mitigation of some optimization methods [35,38], this proposed technique aims to reduce the mean error due to summed variations. This feature is the motivating factor wherein the textural consistency of the portraits varies with multiple semantics. The tampered rate thus possesses either edge or gradient or both variations that must be addressed. The proposed processing technique addresses this problem through independent analysis using deep learning. Therefore, the deep learning paradigm is trained at the low and high levels of its gradient distribution and availability.

3. Textural restoration technique (TRT) using deep feature processing

The design goal of TRT using DFP is to handle and process the degraded periodic artworks through new digital technology for resurrection. The textures and available features of the tampered images are processed, and their gradient distribution is also analyzed based on sequential edge detection for identifying missing gradients. In this textural restoration technique, the missing and available features in the tampered images are considered to improve the textural restoration ratio with filled edges. This technique removes noise by blurring neighboring pixels with similar intensities and outputs in the remaining edges sharp for better reconstruction. Fig. 1 presents the proposed techniques' process in a diagrammatic format.
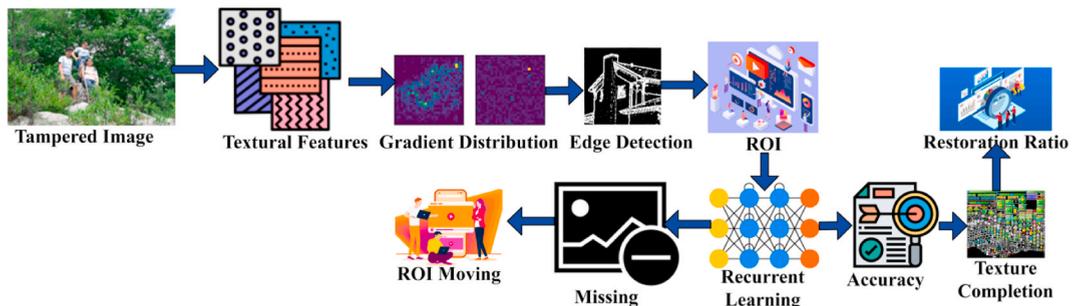
Fig. 1. Proposed TR Technique using Deep Feature Processing Representation.

As presented in Fig. 1, the proposed technique relies on textural features and their gradient distribution from any tampered input. The edges of the textures are identified using their maximum distribution range. From the edge conceded regions, the region of interest (ROI) is extracted upon which the learning operations are pursued. This learning operation provides accurate region detection and texture completion pixels. Besides, the missing distributions are also identified from these regions. As different tampered image processing, the input image textures, features, filled gradients, and missing gradients are varied. However, to retain the ROI from the available features and textures, the proposed technique provides features to fill the gradient for gaining even textures. This textural restoration technique aims to maximize gradient distribution for the unfilled and partial regions using texture pattern classification. The high and low accuracy features are classified and computed between two successive ROIs, resulting in a partial completion edge problem such that this problem reduces gradient distribution and time of filling features, respectively.

Problem Definition: Assume $\{1, 2, ..., tam_{im}\} \in TAM_{IM}$ indicate the set of the tampered images processed in a given time interval $t_{int} \in (F_r - UnF_r + P_r)$. The variables F_r, UnF_r and P_r the filled, unfilled and partial regions are identified from the extracted features near the ROI for gradient distribution. For degraded image processing, the missing gradient M_G is identified using edge detection that is defined in Equation (1):

$$\forall (F_r - UnF_r + P_r), argmin_{M_G} \sum_{i=1}^{t_{int}} (G_D - TF^{ex})_i, t_{int} \in [F_r + 1, UnF_r, P_r]$$

such that

$$G_D = \frac{TF^{ex}}{Edg^D} = maximum \ in \ any(F_r - UnF_r + P) \tag{1}$$

and

$$argmin_{M_G} \sum_{i=1}^{TF^{ex}} (F_r)_i, \forall \{1, 2, ..., tam_{im}\} \in TAM_{IM}, F_r \leq t_{int} \leq UnF_r, P_r$$

in Equation (1), the variable TF^{ex} indicated the textural feature extraction from the input tampered image and $(G_D - TF^{ex})$ is the condition for identifying missing gradients in any region $t_{int} \in [F_r + 1, UnF_r, P_r]$. This increases the sketching of textural edges from the available features near the ROI in different time intervals, reducing the unfilled edges in those images. The process of TRT using DFP-based digital image processing acquires gradient distribution for restoring the unfilled textural features through edge detection (Edg^D) in the given input image. The ancient artworks are processed based on texture pattern classification using recurrent learning (RL) for verifying the gradient substitutions for even textures. The classification output is used for identifying the missing gradients through texture pattern correlation from the ROI, where the combination of missing and available features is initially verified. From the input degraded image, assume k denotes the blur kernel, L^{Img} be the latent image and $\oplus$ indicate the convolution operator. The proposed TRT corresponds to reviving their legacy using digital image processing, and the latent image is expressed in Equation (2)

$$L^{Img} = \frac{1}{t_{int}} \sum_{k}^{t_{int}} (G_D(k)) \oplus tam_{im}(k) \tag{2}$$

where,

$$t_{int}(G^D)_X = \frac{1}{2\pi} \int_{-\infty}^{\infty} \frac{X_k(t_{int})}{M_G(t_{int})} dt_{int \, k-1}$$

$$\tag{3}$$

$$t_{int}(tam_{im})_Y = \frac{1}{2\pi} \int_{-\infty}^{\infty} \frac{Y_k(t_{int})}{M_G(t_{int})} dt_{int \, k-1}$$
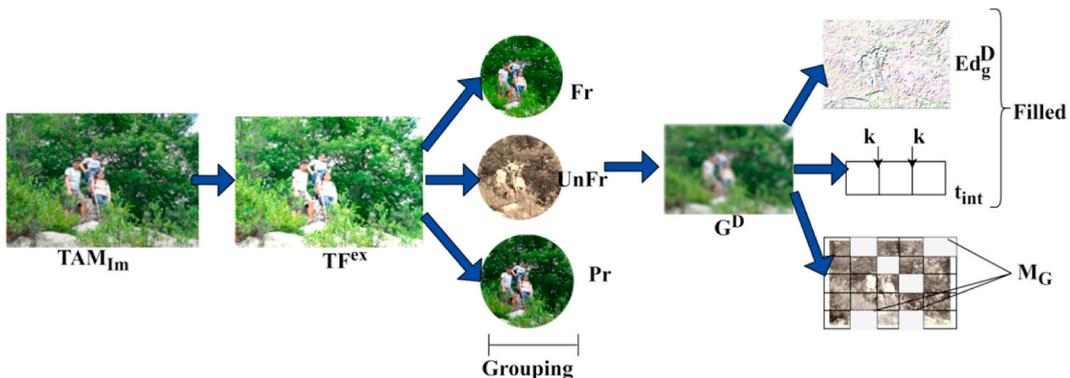
Fig. 2. Gradient distribution and filling process illustration using TF^{ex}.

in Equation (3) $(G^D)_X$ and $(tam_{im})_Y$ used to indicate the phase shift in degraded periodic artworks for the gradient variation in X and Y planes. The variables k and M_G represents the number of blur kernel gradients and missing gradients. In X or Y plane, the rising and falling edges are detected for time t for resurrection, then $X \in [0, \infty]$ and $Y \in [-\infty, 0]$ and hence,

$$t_{int}(G^D)_X = argmin \left\{ \sum_{i-1}^{t_{int}} \frac{(tam_{im} - k \otimes L^{Img})_i}{2N^2} + G^D \sum_{gf} \rho(TF^{ex})_{\max}, t_{int} \in [F_r + 1, UnF_r, P_r] \right. \tag{4}$$

in Equation (4) N^2 denotes the noise variance observed from the input image, gf indicates gradient filters, and $\rho(TF^{ex})_{\max}$ means the probability of maximum textures and available feature extraction. Based on the above instance, the initial noise observation is suppressed using the condition $(tam_{im} - k \otimes L^{Img})$ for the digital image processing to reconstruct and recover ancient artworks and images based on changing X and Y wavelets at given time intervals $(N^2 \times t_{int})$. Here gf_n is the total indexes gradient filtering process performed in this article. The gradient distribution and filling process are illustrated in Fig. 2.

The G^D distribution and filling require the detection of precise overlapping and non-overlapping ROIs. If the regions are overlapping, then G^D distribution is eased using the pixel concentration. In this process, the features extracted and their concentration are maximized through t_{int}. If M_G or $t_{int} \forall k$ is identified, then it is partial/has missing gradients. Therefore, the distribution is required by identifying (moving) ROIs (Fig. 2). The gradient Filtering process controls the noise occurrence in input-tampered images. Noise variance occurs due to the additive spectrum observed in the processing phases regardless of its gradient distribution in any t. This normalization process follows high and low accuracy features based on gradient substitutions through recurrent learning for gaining even textures to reconstruct the tampered image is given in Equations (5) and (6)

$$t_{int}(G^D)_X = \frac{X_k(t_{int})}{M_G(t_{int})} * 2^{\frac{TC^2}{2}} \nabla_i \left[gf_n \times t_{int} - 2^{TC^2} \right]$$

$$t_{int}(tam_{im})_Y = \frac{Y_k(t_{int})}{M_G(t_{int})} * 2^{\frac{TC^2}{2}} \nabla_j \left[gf_n \times t_{int} - 2^{TC^2} \right] \tag{5}$$

where,

$$\nabla_i = f(t_{int}) \left| \frac{TC^2}{2} \right| f(t_{int}) M_{G-1}$$

$$\nabla_j = f(t_{int})^{-1} \left| \frac{TC^2}{2} \right| f(t_{int}) M_{G-1} \tag{6}$$

As per Equations (5) and (6), the features ∇_i and ∇_j are transformed based on high and low accuracy texture gradient distribution for degraded image reconstruction function. The variable $f(t_{int})$ and $f(t_{int})^{-1}$ used to indicate the direct transform and inverse transform functions for ∇_i and ∇_j. Based on the occurrence of the partial and unfilled wavelets (region) X or Y is used for the direct/inverse transform. Such transforms identify the missing gradient to fill the region with high distribution accuracy. The variable TC used for identifying texture completion edge in both X and Y wavelet. Now, the normalized wavelet-based L^{Img} is represented in Equation (7)

$$L^{Img}[f(t_{int})] = \frac{2\frac{TC}{2} \left[(N_2 \times t_{int}) - 2^{gf} \right]}{t_{int}} \times (\nabla_i - \nabla_j)$$

$$such \ that,$$

$$L^{Img}[f(t_{int})] = \frac{2\frac{TC}{2}}{t} \left[\int_0^\infty \frac{\nabla_i \left[(N_2 \times t_{int}) - 2^{gf} \right]}{t_{int}} dt_{int} - \int_{-\infty}^0 \frac{\nabla_j \left[(N_2 \times t_{int}) - 2^{gf} \right]}{t_{int}} dt_{int} \right] \tag{7}$$

This is the normalized wavelet function with less noise variation observed $L^{Img}[f(t_{int})]$ after applying gradient substitutions by moving the ROI. From this condition, the textures and the color combination are extracted for pattern classification. Therefore, the color combination (c_b) and texture (T_e) is computed in Equation (8)

$$c_b = \frac{1}{2\pi (N^2 \times t_{int})} \left\{ \sum_{k=1}^t (X_k - Y_k) M_G \right\}, \forall j = i + 1, i \in gf$$

$$and$$

$$T_e = \sum_{i=\theta_l}^{\theta_h} \Delta \log (c_b)_i \tag{8}$$

where, Δ is the normal plane mapping observation in digital image processing, θ_h and θ_l are the high and low-frequency color combinations observed from the input degraded image. The log normalization output of observing color combination generates T_e for $L^{Img}[f(t_{int})]$ as per Equation (9):

$$T_e[f(t_{int})] = \left(\frac{T_e}{\log\left[\frac{t_{int}}{\theta_h - \theta_l}\right]} \right) \tag{9}$$

This log normalization for sequential gradient distribution is performed to fill the features in any instances and time intervals. The ROI edge detection processes are illustrated in Fig. 3.

The ROI is identified between θ_l and θ_h in the consecutive t_{int}. The ∇_i and ∇_j are convolutional such that it is used for $ROI \in UnF_r$ and P_r extraction. The $[f(t_{int})]$ and $[f(t_{int})]^{-1}$ are concurrently used over ∇_i, ∇_j and $(\nabla_i \oplus \nabla_j)$ for θ_h and θ_l differentiation. This is used for L^{Img} identification from UnF_r and P_r across the ROI (unidentified G^D) observed (Fig. 3). The texture pattern classification is processed based on available features and $T_e[f(t_{int})]$ using recurrent learning. This pattern classification helps to differentiate the true and false positives in the degraded image or both wavelets. In this classification process, the textures and available features are independently analyzed at each level for texture completion edge detection, followed by performing joint classification for texture restoration. First, the input and learning model is trained using gradient distribution accuracy and processed to detect the texture completion edge from the input image. It relies on the c_b and $T_e[f(t_{int})]$ is computed as:

$$DFP[c_b, t_{int}, f(t_{int})] = -\sum_{i=1}^{k} t_{int\,k} - \sum_{j=1}^{k} t_{int\,k} - \sum_{i=1}^{k}\sum_{j=1}^{k} t_{int\,k} edg_i$$

and

$$I[c_b, t_{int}] = \frac{(M_G)^{DFP[c_b, t_{int}, f(t_{int})]}}{\sum_{t=1}^{N^2 \times t_{int}} (M_G)^{DFP[c_b, t_{int}, f(t_{int})]_i}} \tag{10}$$

in Equation (10), $DFP[.]$ denotes the deep feature processing of c_b and $I[.]$ is the initial training model at t interval. Where, edg_i is the texture completion edge identified between two successive ROIs. Similarly, the learning model is initially trained using the analysis of gradient distribution to fill the missing region is given as:

$$FP\left[T_e\left[f(t_{int})\right]\right], c_b = \begin{cases} \sum_{t=1}^{t} t_{int\,k} edg_i \frac{1}{\nabla_i}, & \text{if } X_k(t_{int}) \in [0, \infty] \\ \sum_{t=1}^{t} t_{int\,k} edg_i \nabla_j, & \text{if } X_k(t_{int}) \notin [0, \infty] \end{cases} \tag{11}$$

$$I[T_e[f(t_{int})]] = \frac{(M_G)^{DFP[T_e[f(t_{int})], c_b]}}{\sum_{t=1}^{t} (M_G)^{DFP[T_e[f(t_{int})], c_b]}}$$

in Equation (11) the missing gradient and joint visible are analyzed through recurrent learning such that $DFP[T_e[f(t_{int})], c_b]$ is computed for both the accuracy gradient distribution/wavelets. This process helps to differentiate the transform and frequency of the degraded image in t to facilitate possible texture pattern classification from the instances. The RL for accuracy classification is presented in Fig. 4.

The above representation is different from conventional recurrent learning using the classification process. The classification is distinct from multiple gradient layers for the available K. However, this differs from the conventional feedforward network by performing classifications of identified and missing. The first classification is performed for (X_k, Y_k) identification through $f(t_{int})$ alone. Here, ∇_i and $(\nabla_i \oplus \nabla_j)$ are cumulatively processed using $f(t_{int})$ for precise identification. Different from this, if T_e is the achievable output at any k, then $f(t_{int})^{-1}$ generates Y_k alone stating that G^D is missing in some ROI (Refer to Fig. 4). The missing gradient is separated by ROI, and available feature processing relies on $L^{Img}[f(t_{int}) \in [-\infty, \infty]$ for the wavelets $X_k \in [0, \infty]$ or $Y_k \notin [0, \infty]$. In this case, $X_k \notin [0, \infty]$ is used to achieve a gradient of $[-\infty, 0]$ that indirectly indicates Y_k at any instance. Therefore, the gradient of the input image is independently analyzed using $I[.]$, whereas in the learning model is training $I[.]^*$ for the missing texture restoration, and hence,
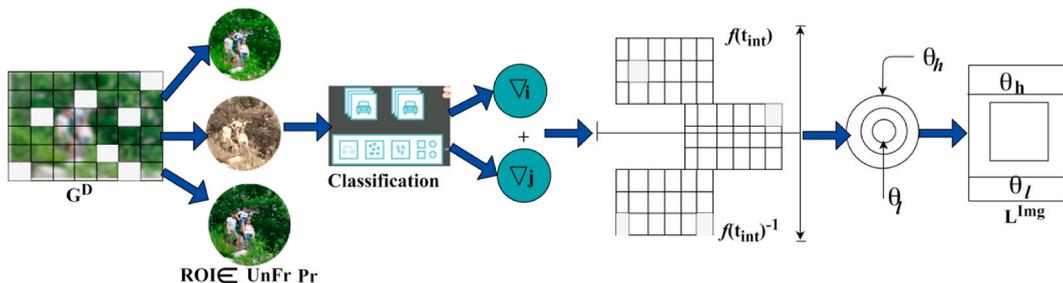
Fig. 3. ROI edge detection process using G^D.

the previous $I[.]$ does not handle further processing and verification. From the sequence, $X_k \notin [0,\infty]$ is detected as the false positives/partial region, whereas $Y_k \notin [0,\infty]$ is fulfilled gradient region, here $X_k \in [0,\infty]$ and $X_k \notin [0,\infty]$ is considered for identifying gradient missing region. These false positives FP are computed with the direct and inverse transform to require the final result ($\exists$). Hence, the sequential computation of the gradient missing region is represented as $\{M_{G_1}$ to $M_{G_{N^2 \times t_{int}}}\}$ for both the high and low gradient distribution, accuracy inputs are estimated. The missing gradient identification along with texture completion edge detection edg is computed as:

$$\left. \begin{aligned} M_{G_1} &= L^{Img}[f(1)] \\ M_{G_2} &= L^{Img}[f(2)] - \frac{edg_1}{(M_G)^{DFP[c_b,\,t_{int}\,f(t_{int})]_1}} \\ &\vdots \\ M_{G_{N^2 \times t_{int}}} &= L^{Img}\left[f\left(N^2 \times t_{int}\right)\right] - \frac{edg_{N^2 \times (t_{int}-1)}}{(M_G)^{DFP[c_b,\,t_{int}\,f(t_{int})]_{N^2 \times t_{int}}}} \end{aligned} \right\} , \forall tam_{im} = t_{int}\left(G^D\right)_X + t_{int}\left(G^D\right)_Y \tag{12}$$

Such that,

$$\left. \begin{aligned} M_{G_1} &= L^{Img}\left[f(1)\right] - edg_{\nabla-1} \times DFP[I[T_e[f(t_{int})]], c_b]_{\nabla-1} \\ M_{G_2} &= L^{Img}\left[f(2)\right] - edg_{\nabla} \times DFP[I[T_e[f(t_{int})]], c_b]_{\nabla} \\ &\vdots \\ M_{G_{N^2 \times t_{int}}} &= L^{Img}\left[f\left(N^2 \times t_{int}\right)\right] - edg_{N^2 \times t_{int}} \times DFP[I[T_e[f(t_{int})]], c_b]_{N^2 \times t_{int}} \end{aligned} \right\} , \forall L^{Img} = t_{int}\left(G^D\right)_X + t_{int}\left(G^D\right)_Y \tag{13}$$

Based on Equations (12) and (13), ∇ is the point at which the texture pattern classification is distinguished with the condition $tam_{im} = t_{int}(G^D)_X + t_{int}(G^D)_Y$ for X or Y plane. In this point of separation of ROI, the time and missing gradient are the important factors in identifying the precise gradient distribution accuracy. This is because, of the variation in available features and the combination of missing ones, the ROI is marked for sketching accurate textural edges in different time instances based on texture pattern classification. The point on X and Y plane indicates the varying gradient distribution accuracy such that if $M_{G_{N^2 \times t_{int}}} \notin t_{int}(G^D)_X$ or $M_{G_{N^2 \times t_{int}}} \in t_{int}(G^D)_X \leq \nabla < M_{G_{N^2 \times t_{int}}} \in (X+Y)$ is the precise output for classification. If the current instance does not satisfy the above condition, then the false positive increases by one, and the ROI moves to fill the missing gradient. In other words, the condition $M_{G_{N^2 \times t_{int}}} \notin t_{int}(G^D)_X$ is observed in any instance, if $FP = FP + 1$ is achieved else, true positive $TP = TP + 1$ is achieved. The RL for missing G^D classification is presented in Fig. 5.

The classification $\forall M_{G_N}$ relies on edg_i identified under $\Delta = 0$ and $\Delta = 1$ such that (X,Y), (X), and (Y) are the individual outputs. The M_{G_N} identified from $\Delta = 1$ is the precise FP due to which the classification is split. In this splitting $[(X,Y)|(X)]$ and $[(Y)]$ are independently handled for identifying ROI displacements (Fig. 5). In texture pattern classification, it is necessary to improve the true positives other than the texture and available features. For this computation, independent and joint gradient distribution is induced for all the texture completion edge detection. The deviation between the direct/inverse transform analysis helps to compute the identification of FP and TP to fill the missing edges. If any overlap occurs in this iteration, then $FP = FP + 1$, and this computation is consolidated for the time interval. In this TRT model, digital image processing is used to verify the gradient distribution accuracy considering the missing gradient positions, achieving maximum restoration. The analyses of UnF_r and P_r classification throughout edg_i under the varying features are presented in Fig. 6(a) and (b)

The UnF_r and P_r vary with the detected edg_i and TF. This is due to the improvements in $I[.]$ from various iterations using θ_h and θ_l. This forms L^{Img} by increasing the chances of (X_k, Y_k) (alone) detection. Therefore the new $I[.]$ imposes $f(t_{int})$ alone for identifying ROIs across multiple G^D. Regardless of the missing G^D, the gl_n estimated from the previous t are used for T_e balancing. This aids in identifying Y_k between successive iterations. The instances where Y_k is alone identified causes FP and therefore P_r is extracted (Fig. 6(a) and (b)). Pursued by the (X_k, Y_k), (X_k), and (Y_k) alone, the FP analyses for the increasing iterations are discussed in Fig. 7.
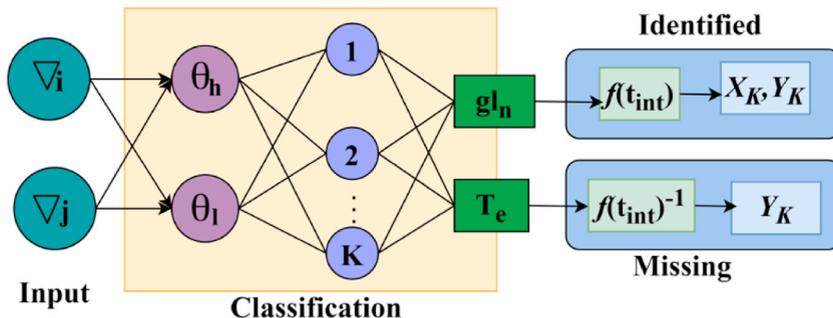
Fig. 4. RL for accuracy classification between "identified" and "missing" gradients.
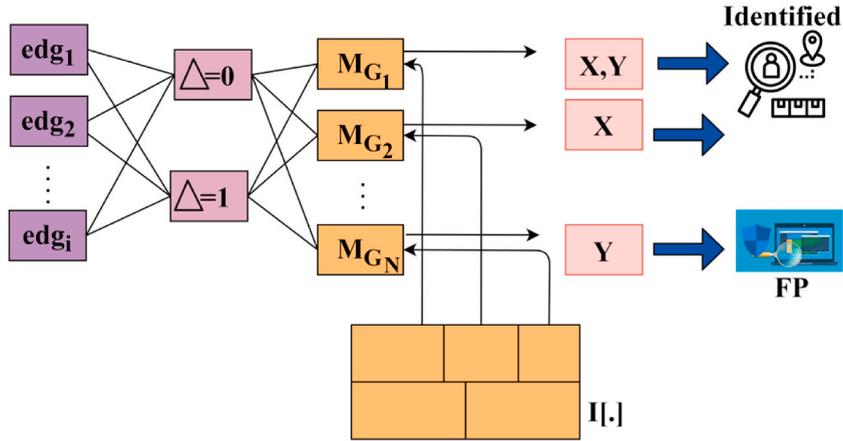
Fig. 5. RL for missing G^D classification using different edges.

The false positives are confined at a high rate $\forall X_k$ compared to (X_k, Y_k) and (Y_k). This is due to the k mitigation by distributing $f(t_{int})$ and $f(t_{int})^{-1}$ outputs in P_r other than Edg^D regions. Based on the available combinations of X_k and Y_k the FP reduction is performed. In case of Δ_i and Δ_j based analyses, the FP is less for $(\nabla_i \oplus \nabla_j)$ for $ROI \in UnF_r$ and P_r alone. This is used for $I[.]$ where $\Delta = 0$ and $\Delta = 1$ are comparatively used for identifying FP. If such FP is identified, then the nearest ROI is moved across for G^D, reducing the FP (Refer to Fig. 7(a) and (b).

4. Experimental assessment

The experimental assessment considers the stored tampered and original images from the source "https://www.kaggle.com/datasets/saurabhshahane/cg1050" [42]. This source provides 730 original images for training and validation. Another variant provides 314 images for training and testing. The first provides images with 80–240 pixels, and the second provides 180 to 720 pixels. One sample image from the above dataset is analyzed using MATLAB experiments. The results are presented in Tables 2–4.

The comparative assessment considers the metrics of accuracy, sensitivity, restoration ratio, mean error, and classification time. The ROI varied between 1 and 11, and the features varied between 2 and 28 for their impact analysis. The analysis is performed
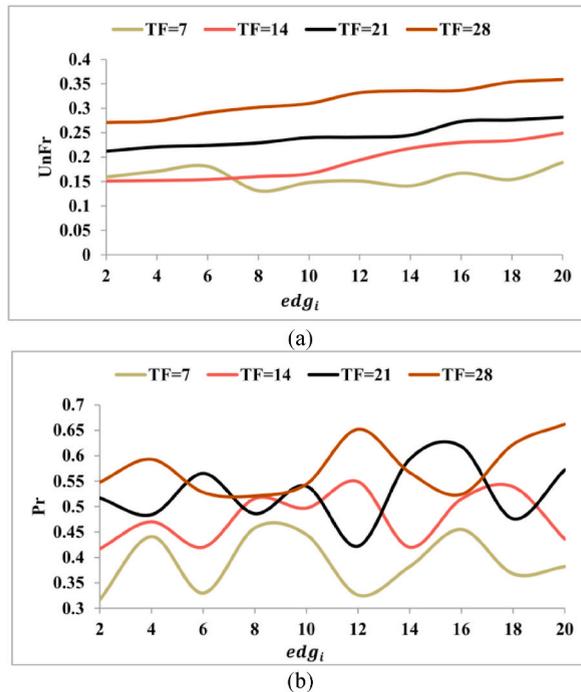
Fig. 6. (a) UnF_r and (b) P_r classification analysis.

(a)

(b)
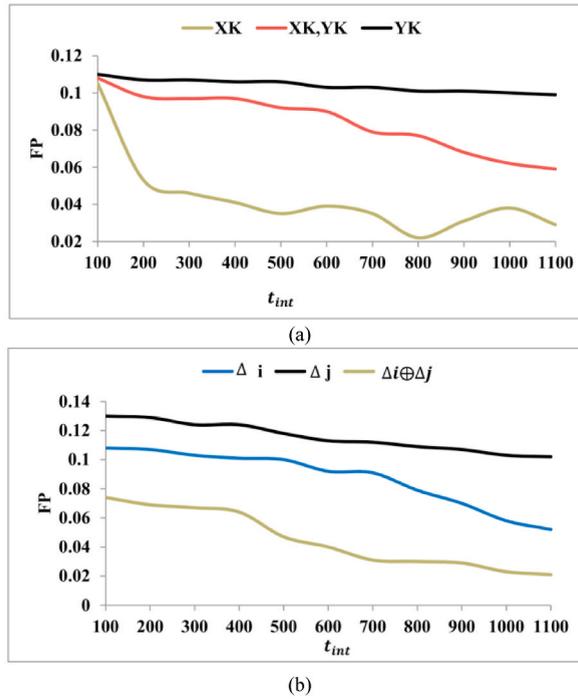
Fig. 7. Fp analyses for t_{int}.

alongside the existing methods: ADNL [29], SASL [36], and NCTVM [38].

4.1. Accuracy

The deep feature processing of degraded ancient artworks and images is reconstructed to gain accurate images. It satisfies high gradient distribution accuracy using the proposed TRT (Refer to Fig. 8(a) and (b)). The missing gradient and false positive occurred in image processing due to noise variations in degraded image processing at different time intervals. The textures and available features are extracted in these ancient image reconstruction processes to revive their legacy. The identified features provide a wide knowledge of their patterns and gradients. The textural pattern classification is performed using recurrent learning and processing the final output image for X and Y plane for separating filled and unfilled gradients from the input image. The precise degraded image processing relies on texture and available feature extraction using high and low accuracy features separated for reducing partial gradient distribution. The textural features are extracted through deep feature processing to verify the gradient substitutions for even textures based on the normalized wavelet finding unfilled regions in a given input, preventing error. Therefore, the gradient feature accuracy is less in this proposed technique.

Table 2
Gradient distribution.

Input	UnF_r	P_r

Table 3
Edge detection.

k Output	edj_i	Edg^D
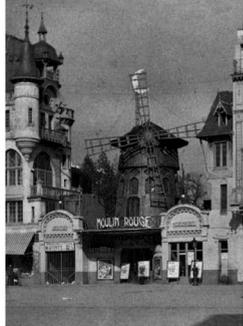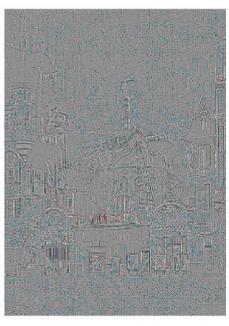
Table 4
Restoration.

$I[.]$	Output
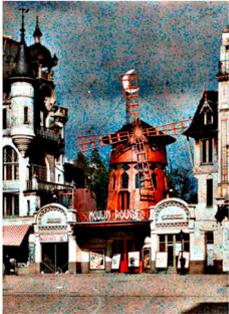
4.2. Sensitivity

This proposed technique satisfies a high sensitivity rate for reliable degraded image processing based on restoring the textural feature extraction to denote the missing gradients is reduced to speed up the decision-making for pattern classification is depicted as (Refer to Fig. 9(a) and (b)). The ROI near missing gradient is identified from the available features and controlling unfilled edges and then distribute gradient to that region through moving ROI. The missing problem is mitigated from their gradient for both wavelets with precise feature selection to optimize the extracted textural features. The orientation, color combination, and texture of degraded images are increased with the help of deep feature processing for training the learning model. Based on the image processing, the high and low filtering features are exhibited and compared with an existing dataset to easily identify missing gradients for moving ROI. This continuous degraded image processing maximizes sensitive information handling at a similar time of training the learning model. If any false positive occurs in image processing, it is continuously monitored to achieve maximum sensitivity. Hence, the textural completion edge satisfies high accuracy features for gradient distribution, reducing error in those regions.

4.3. Restoration ratio

In this proposed technique, the textural edges are sketched for moving the ROI based on gradient distribution to that region, which is analyzed through recurrent learning and comparing current degraded image-sensitive data with an existing image for similarity analysis (Refer to Fig. 10(a) and (b)). The initial learning model is trained for verifying the gradient distribution and achieves high textural feature restoration ratio in this article compared to the other factors. In this technique, the sequential feature orientation is analyzed and verified; the gradient is substituted in the unfilled region to generate a gradient-filled region for X, or Y is used for functions of the transform. This transform analysis is performed to identify missing gradients from the available features with high accuracy of gradient distribution for restoring even textures. By training the learning process, the partial/unfilled region is reduced using Equations (8)–(10) computation. This proposed technique separates the high and low accuracy features to identify false positives and prevent errors. Therefore, this false positive is controlled by the sequential gradient distribution, and it achieves maximum
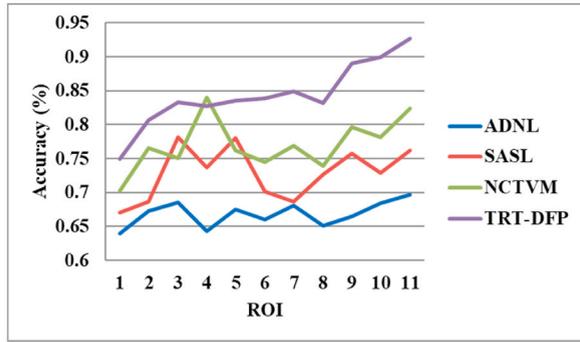
(a)
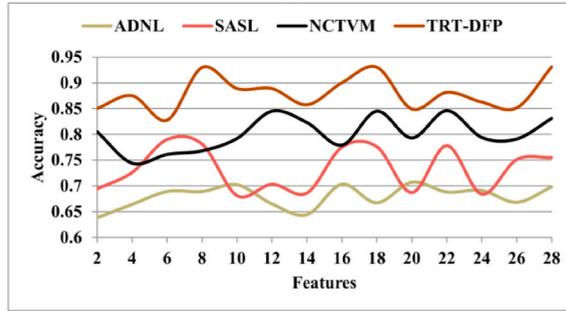
(b)

Fig. 8. Accuracy comparisons for (a) ROI and (b)Features.
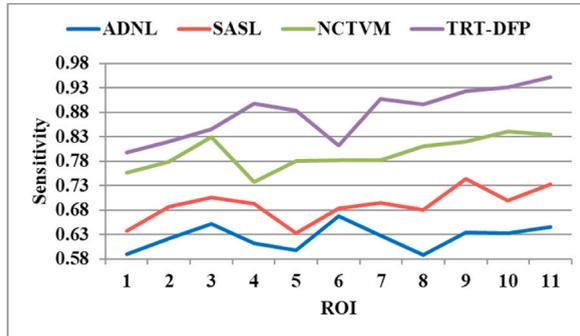
(a)
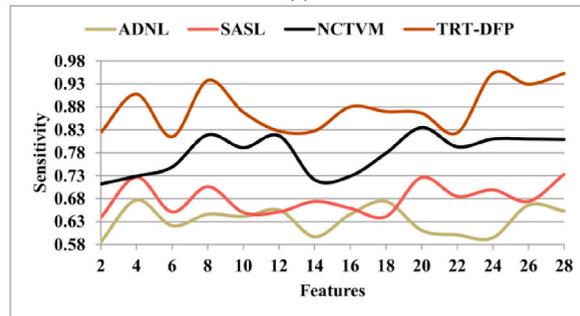
(b)

Fig. 9. Sensitivity comparisons for (a) ROI and (b) features.
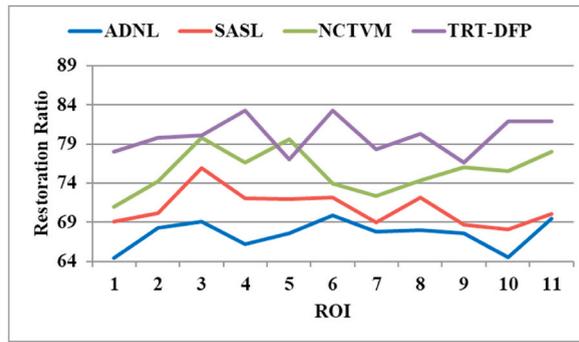
(a)
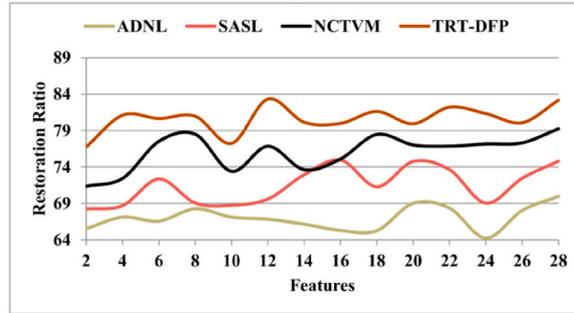
(b)

Fig. 10. Restoration ratio comparisons for (a) ROI and (b) features.
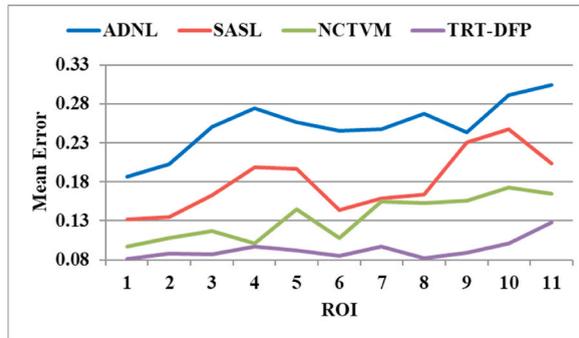
(a)
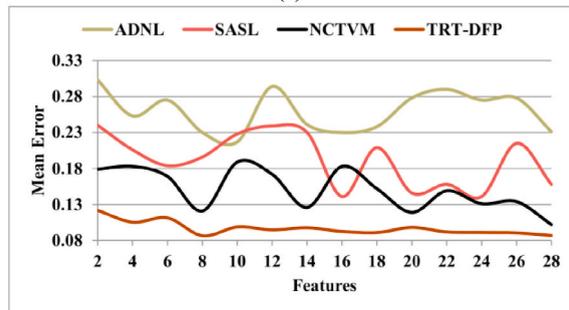
(b)

Fig. 11. Mean error comparisons for (a) ROI and (b) features.

restoration.

4.4. Mean error

In Fig. 11(a) and (b), the mean error identified in the proposed technique during textural pattern classification is considerably less than the gradient distribution and texture completion edge detection. The edge detection at the first level is used for identifying the missing gradient based on stored input analysis for the initial image processing output. This gradient distribution is performed for even texture arrangement, and modifying color combination, brightness, and textures helps to process accurate pattern classification and edge detection. After the classification process, the gradient-filled, partially filled, and unfilled region is verified based on the texture pattern classification, and its edge detection is performed for the single or multiple images, preventing mean errors. The variations in textural features are identified using accurate and appropriate pattern classification with a combination of missing for marking ROI. This classification is performed using recurrent learning for training the learning model for textural completion edge detection. This classification helps to reduce the false positive with an increasing true positive ratio for all the sequences, reducing mean error in this proposed technique.

4.5. Classification time

In this proposed technique, the textures and available features are independently analyzed at each level for detecting the texture completion edge, followed by performing joint classification for restoration. Through learning model training and texture, the completion edge does not change its color combination, texture, and orientation. The noise variation relies on the texture pattern classification based on $L^{Img}[f(t_{int}) \in [-\infty, \infty]$ for the wavelets $X_k \in [0, \infty]$ or $Y_k \notin [0, \infty]$. The above condition is analyzed for the first gradient distribution for maximum restoration. From the sequence, the textural edge is detected as the false positives/partial region, whereas the maximum accuracy feature is fulfilled by the gradient region for preventing errors. For both the high and low gradient distribution accuracy identified from the instance, the feature changes and noise variation are compared with the existing dataset for TRT. Hence, in this proposed technique, the filled textural features and their gradient positions are marked for moving the ROI to precisely distinguishing textures through recurrent learning and achieving less classification time, as represented in Fig. 12(a) and (b). Tables 5 and 6 present the comparative analysis summary of the ROIs and features.

In addition, the efficiency of the system is evaluated using different metrics such as Peak Signal Noise Ratio (PSNR), Structural Similarity Index Metrics (SSIM), and Frechlet Inception Distance (FID). The obtained results are illustrated in Table 7.

Table 7 illustrates that the proposed TRT-DFP method attains high PSNR value, SSIM, and minimum FID, which indicates that the system attains effective image restoration while analyzing various ROI regions compared to other methods.

(a)

(b)
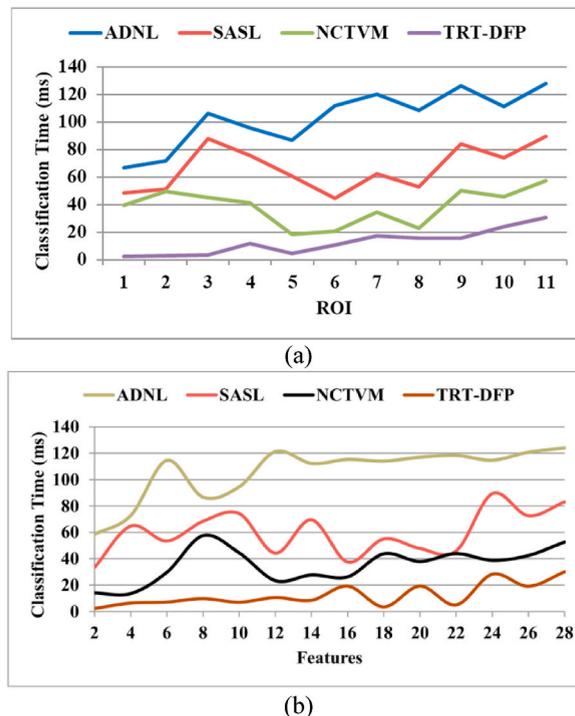
Fig. 12. Classification time comparisons for (a) ROI and (b) features.

Table 5
Comparative analysis summary (ROI).

Metrics	ADNL	SASL	NCTVM	TRT-DFP
Accuracy	0.697	0.762	0.824	0.9268
Sensitivity	0.645	0.732	0.834	0.9523
Restoration Ratio	69.46	70.08	78.04	81.917
Mean Error	0.304	0.204	0.165	0.1279
Classification Time (ms)	128.03	89.71	57.35	30.595

The proposed technique improves accuracy, sensitivity, and restoration ratio by 8.29 %, 10.77 %, and 9.39 %. This proposed technique reduces mean error and classification time by 9.64 % and 11.11 %.

Table 6
Comparative analysis summary (features).

Metrics	ADNL	SASL	NCTVM	TRT-DFP
Accuracy	0.698	0.755	0.831	0.9312
Sensitivity	0.653	0.733	0.809	0.9528
Restoration Ratio	69.96	74.81	79.24	83.169
Mean Error	0.231	0.158	0.102	0.0868
Classification Time (ms)	124.08	83.14	52.64	29.954

The proposed technique improves accuracy, sensitivity, and restoration ratio by 8.49 %, 11.06 %, and 8.5 %. This proposed technique reduces mean error and classification time by 7.69 % and 10.9 %.

Table 7
Comparative analysis summary (ROI).

Metrics	ADNL	SASL	NCTVM	TRT-DFP
PSNR	45.3	48.99	53.78	65.33
SSIM	0.673	0.734	0.823	0.967
FID	0.56	0.468	0.328	0.124

5. Summary

This article discussed the process and functions of textural restoration techniques using deep feature processing for leveraging the quality of tampered art designs. This technique relies on textural feature extraction and classification at the pre-initial steps. In the later processing, the region of interest is identified and classified based on gradient distribution. Deep recurrent learning is used for classifying accurate distributions for restoration and missing gradient regions. The different region of interest combinations using the textural features are used for detecting the internal edges of a tampered old image. The edges are filled with pixel gradients by reducing the noise. The textural patterns are classified as low and high-accuracy gradients for which substitutions and moving are validated using the learning paradigm. Further gradient distribution and edge completion are recommended depending on the learning output. Similarly, if the distributed gradients are enough to fill the partial or non-distributed edges, the completion is pursued with the previous positions' gradients. This improves the restoration ratio with a marked region of interest under different textures. The proposed technique improves accuracy, sensitivity, and restoration ratio by 8.49 %, 11.06 %, and 8.5 %. This proposed technique reduces mean error and classification time by 7.69 % and 10.9 %. Though the proposed technique is better at improving the classification accuracy, the problem of descendant gradients remains unresolved in the edge detection process. This requires texture completion verification using reference pixels. Additionally, when the texture data to be processed is complicated the texture data resulting from the algorithms is comparatively blurred and fails to reflect the texture structure of the originalimage. This is because of the limitations in matching block searching and texture dispersion during large-area restoration. Blurring of the corrected area and insufficient texture information in areas with complex texture and substantial missing texture are two limitations of the present study. Therefore, future work will incorporate single/multi-reference pixels for precise edge descendant detection.

Patient consent statement

Not applicable.

Permission to reproduce material from other sources

Not applicable.

Clinical trial registration

Not applicable.

Data availability statement

Question: Has data associated with your study been deposited into a publicly available repository?
Response: No.
Question: Please select why. Please note that this statement will be available alongside your article upon publication.
Response: Data will be made available on request.

CRediT authorship contribution statement

Guo Chen: Conceptualization, Methodology, Writing – original draft, Writing – review & editing. **Zhiyong Wen:** Data curation, Investigation, Writing – review & editing. **Fazhong Hou:** Investigation, Validation, Writing – review & editing.

Declaration of competing interest

The authors declare that they have no known competing financial interests or personal relationships that could have appeared to influence the work reported in this paper.

References

[1] X. Wei, 3D landscape art design and network space reconstruction based on complex embedded system, Microprocess. Microsyst. 80 (2021), 103539.
[2] H. Liu, Y. Xu, F. Chen, Sketch2Photo: synthesizing photo-realistic images from sketches via global contexts, Eng. Appl. Artif. Intell. 117 (2023), 105608.
[3] W. Li, Y. Wang, Y. Su, X. Li, A. Liu, Y. Zhang, Multi-scale fine-grained alignments for image and sentence matching, IEEE Trans. Multimed. 25 (2023) 543–556.
[4] G. Demir, A. Çekmiş, V.B. Yeşilkaynak, G. Unal, Detecting visual design principles in art and architecture through deep convolutional neural networks, Autom. ConStruct. 130 (2021), 103826.
[5] P. Baglioni, D. Chelazzi, R. Giorgi, Nanorestart: nanomaterials for the restoration of works of art, Heritage Science 9 (2021) 1–5.
[6] K. Wu, X.M. Fu, R. Chen, L. Liu, Survey on computational 3D visual optical art design, Visual Computing for Industry, Biomedicine, and Art 5 (1) (2022) 1–31.
[7] Y. Guo, The microscopic visual forms in architectural art design following deep learning, J. Supercomput. 78 (1) (2022) 559–577.
[8] R. Cong, H. Sheng, D. Yang, Z. Cui, R. Chen, Exploiting spatial and angular correlations with deep efficient transformers for light field image super-resolution, IEEE Trans. Multimed. (2023), https://doi.org/10.1109/TMM.2023.3282465.
[9] Q. Liu, H. Yuan, R. Hamzaoui, H. Su, J. Hou, H. Yang, Reduced reference perceptual quality model with application to rate control for video-based point cloud compression, IEEE Trans. Image Process. 30 (2021) 6623–6636.
[10] A. Bugeja, M. Bonanno, L. Garg, 3D scanning in the art & design industry, Mater. Today: Proc. 63 (2022) 718–725.
[11] C. Tang, Application of internet thinking in the teaching of environmental art design, Microprocess. Microsyst. 81 (2021), 103712.
[12] R.A. Alves, K. Strecker, R.B. Pereira, T.H. Panzera, Mixture design applied to the development of composites for steatite historical monuments restoration, J. Cult. Herit. 45 (2020) 152–159.
[13] T. Lu, K. Zhao, Y. Wu, Z. Wang, Y. Zhang, Structure-texture parallel embedding for remote sensing image super-resolution, Geosci. Rem. Sens. Lett. IEEE 19 (2022) 1–5.
[14] Z. Zhang, H. He, A customized low-rank prior model for structured cartoon–texture image decomposition, Signal Process. Image Commun. 96 (2021), 116308.
[15] J. Deng, X. Zhang, H. Chen, L. Wu, BGT: a blind image quality evaluator via gradient and texture statistical features, Signal Process. Image Commun. 96 (2021), 116315.
[16] C. Fu, H. Yuan, H. Xu, H. Zhang, L. Shen, TMSO-Net: texture adaptive multi-scale observation for light field image depth estimation, J. Vis. Commun. Image Represent. 90 (2023), 103731.
[17] J. Zhang, C. Zhu, L. Zheng, K. Xu, ROSEFusion: random optimization for online dense reconstruction under fast camera motion, ACM Trans. Graph. 40 (4) (2021) 56.
[18] O. Kodym, M. Hradiš, TG 2: text-guided transformer GAN for restoring document readability and perceived quality, Int. J. Doc. Anal. Recogn. 25 (1) (2022) 15–28.
[19] C. Wang, L. Xu, L. Liu, Structure–texture image decomposition via non-convex total generalized variation and convolutional sparse coding, Vis. Comput. 39 (2022) 1121–1136.
[20] H. He, L. Zhao, A doubly sparse and low-patch-rank prior model for image restoration, Appl. Math. Model. 112 (2022) 786–799.
[21] B. Su, X. Liu, W. Gao, Y. Yang, S. Chen, A restoration method using dual generate adversarial networks for Chinese ancient characters, Visual Informatics 6 (1) (2022) 26–34.
[22] B. Hu, S. Wang, L. Li, J. Leng, Y. Yang, X. Gao, Hierarchical discrepancy learning for image restoration quality assessment, Signal Process. 198 (2022), 108595.
[23] P. Zhu, Z. Gao, C. Xie, Multiframe blind restoration with image quality prior, Appl. Soft Comput. 120 (2022), 108632.
[24] M. Hassan, Y. Wang, D. Wang, W. Pang, K. Wang, D. Li, D. Xu, Restorable-inpainting: a novel deep learning approach for shoeprint restoration, Inf. Sci. 600 (2022) 22–42.
[25] B. Hu, L. Li, J. Wu, J. Qian, Subjective and objective quality assessment for image restoration: a critical survey, Signal Process. Image Commun. 85 (2020), 115839.

[26] W. Xu, Y. Fu, Deep learning algorithm in ancient relics image colour restoration technology, in: Multimedia Tools and Applications, 2022, https://doi.org/10.1007/s11042-022-14108-z.

[27] M.E. Hatir, I. Ince, Lithology mapping of stone heritage via state-of-the-art computer vision, J. Build. Eng. 34 (2021), 101921.

[28] Z. Jin, M.Z. Iqbal, D. Bobkov, W. Zou, X. Li, E. Steinbach, A flexible deep CNN framework for image restoration, IEEE Trans. Multimed. 22 (4) (2019) 1055–1068.

[29] J. Yuan, Z. He, Adversarial dual network learning with randomized image transform for restoring attacked images, IEEE Access 8 (2020) 22617–22624.

[30] Z. Xue, Q. Xu, M. Zhang, Local transformer with spatial partition restore for hyperspectral image classification, IEEE J. Sel. Top. Appl. Earth Obs. Rem. Sens. 15 (2022) 4307–4325.

[31] Z. Wan, B. Zhang, D. Chen, P. Zhang, F. Wen, J. Liao, Old photo restoration via deep latent space translation, IEEE Trans. Pattern Anal. Mach. Intell. 45 (2) (2022) 2071–2087.

[32] N. Farajzadeh, M. Hashemzadeh, A deep neural network based framework for restoring the damaged Persian pottery via digital inpainting, Journal of Computational Science 56 (2021), 101486.

[33] C. Li, B. Sun, L. Tang, A non-convex hybrid regularization model for restoring blurred images with mixed noises, Digit. Signal Process. 130 (2022), 103734.

[34] H. Chen, Z. Xu, Q. Feng, Y. Fan, Z. Li, An L0 regularized cartoon-texture decomposition model for restoring images corrupted by blur and impulse noise, Signal Process. Image Commun. 82 (2020), 115762.

[35] W. Wang, C. Su, An optimization method for motion blur image restoration and ringing suppression via texture mapping, ISA Trans. 131 (2022) 650–661.

[36] F. Wu, W. Dong, T. Huang, G. Shi, S. Cheng, X. Li, Hybrid sparsity learning for image restoration: an iterative and trainable approach, Signal Process. 178 (2021), 107751.

[37] S. Lee, M. Kang, Group sparse representation for restoring blurred images with Cauchy noise, J. Sci. Comput. 83 (2020) 1–27.

[38] M. Kang, M. Jung, Simultaneous image enhancement and restoration with non-convex total variation, J. Sci. Comput. 87 (3) (2021) 83.

[39] S.W. Zamir, A. Arora, S. Khan, M. Hayat, F.S. Khan, M.H. Yang, Restormer: efficient transformer for high-resolution image restoration, in: Proceedings of the IEEE/CVF Conference on Computer Vision and Pattern Recognition, 2022, pp. 5728–5739.

[40] Z. Wang, X. Cun, J. Bao, W. Zhou, J. Liu, H. Li, Uformer: a general u-shaped transformer for image restoration, in: Proceedings of the IEEE/CVF Conference on Computer Vision and Pattern Recognition, 2022, pp. 17683–17693.

[41] P. Kumar, V. Gupta, Restoration of Damaged Artworks Based on a Generative Adversarial Network. *Multimedia Tools And Applications*, 2023, https://doi.org/10.1007/s11042-023-15222-2.

[42] https://www.kaggle.com/datasets/saurabhshahane/cg1050.